CrossMark

Synthesis and systematic investigations of Al and Cu-doped ZnO nanoparticles and its structural, optical and photo-catalytic properties

S. Kumaresan[1] · K. Vallalperuman[2] · S. Sathishkumar[1] · M. Karthik[1] ·
P. SivaKarthik[3]

Abstract Here we report, copper (Cu) and Aluminum (Al) doped zinc oxide (ZnO) nanoparticles by a novel one step microwave irradiation method for the first time. Powder X-ray diffraction (XRD) reveals that both pure and doped samples assigned to hexagonal wurtzite type structure. The calculated average crystalline size decreases from 24 to 11 nm for pure and doped (Al and Cu) ZnO respectively, which is in good agreement with the particles size observed from Transmission Electron Microscope (TEM) analyses. A considerable red shift in the absorption edge and the reduction in the energy gap from 3.35 to 2.95 eV reveal the substitution of Al^{3+} and Cu^{2+} ions into the ZnO lattice analyzed by UV–Vis transmission spectra. The photocatalytic degradation of Methyl Violet (MV), Phenol and Rhodamine B (RHB) was investigated by using pure, Al and Cu doped ZnO catalyst under UV light irradiation. The results showed that the photocatalytic property is significantly improved by Cu doping concentration. This could be attributed to extended visible light absorption, inhibition of the electronhole pair's recombination and enhanced adsorptivity of dye molecule on the surface of Cu–ZnO nanopowders. The samples were further characterized by photoluminescence spectra and Fourier Infrared Spectra (FTIR) analysis.

✉ K. Vallalperuman
  vallalphysics1@gmail.com

1   Research and Development Centre, Bharathiar University, Coimbatore 640 046, Tamilnadu, India

2   Department of Physics, Thiru Kolanjiappar Government Arts College, Vriddhachalam 606 001, Tamilnadu, India

3   Department of Chemistry, University College of Engineering, Panruti 607 106, Tamilnadu, India

1 Introduction

Wide band-gap oxide semiconductors, when doped with transition metal ions have attracted much attention for their promising versatile applications. Heterogeneous photocatalytic decomposition of organic pollutants is one of the most promising processes for air and water decontamination. Further, semiconductor spirited heterogeneous photocatalysis using various functional nanomaterials are intensively studied for the degradation of several recalcitrant compounds in the aqueous medium and gaseous phase under UV/visible light. TiO_2, ZnO and WO_3 [1–4], nanoparticles are the quintessential photocatalyst, a material that allows a reaction to happen in the presence. Loaded with a metal cocatalyst (Al, Cu, Pd, Pt, Rh), both rutile and anatase [5–7] nanoparticles catalyze the overall splitting of water into molecular hydrogen and oxygen when illuminated with ultraviolet light. Among the various types of metal oxide semiconductors, ZnO is one of the technologically important semiconductors and has been widely used as a photocatalyst because of its large area-to-volume ratio, direct wide band gap (3.37 eV), high photosensitivity, low cost and high chemical stability [8, 9]. One of the major drawbacks is rapid electron/hole recombination of pure ZnO in the photocatalytic process, which is faster than the surface redox reactions and limits the photodegradation reaction under normal conditions [10, 11]. Many studies have been reported to prevent recombination of electron/hole pairs and improve photocatalytic activity of ZnO, such as using ZnO with noble metals (e.g., Au, Ag, Pt, or Pd) [12–15], metals (Fe, Mg, Ca and Al) [16].

Hence, in the present work, the authors have chosen two metal ion dopants such as Al and Cu to load with ZnO in order to increase the photocatalytic property. Many methods have been adapted to synthesis of ZnO nanostructures

such as, non-aqueous approaches, chemical-precipitation, sol–gel process, gas condensation, hydrothermal process, aerosol spray process, and hydrolysis in polyol medium. When compare with the above mentioned methods, the microwave irradiation method has sparked much interest due to their operation simplicity, effective, low-cost route to synthesis, less time consuming (about 10 min), and for large-scale production [17]. Therefore, it is aimed to synthesis Al and Cu doped ZnO nanoparticles by simple household microwave irradiation method. The effect of dopants on structural, morphological, optical and photocatalytic properties of ZnO nanoparticles has been systematically investigated. To the best of the author's knowledge, this is the first preliminary report about photocatalytic properties of Al and Cu doped ZnO nanoparticles by microwave irradiation method.

2 Experimental procedure

2.1 Materials

Zinc chloride dihydrate ($ZnCl_2·2H_2O$), copper chloride dihydrate ($CuCl_2·2H_2O$), aluminum chloride ($AlCl_3$) was purchased from Sigma-Aldrich (purity 99.97%). Ethanol, NH_4OH, Methyl violet, (MV), Phenol, Rhodamine B (RhB) dyes were purchased from Merck. As all these chemicals are Analytical Grade, they were used without further purification.

2.2 Preparation of Al–Cu–ZnO photocatalyst

Pure and Al–Cu–ZnO nanopowders were prepared by microwave irradiation method. Initially, 0.1 M solution of zinc hydroxyl group was prepared by mixing of 2.5 g $ZnCl_2$ with 100 ml of double distilled water. Appropriate amount (5 wt.%) of $AlCl_3$ and $CuCl_2·2H_2O$ was added in the zinc hydroxyl group solution with continuous stirring using a magnetic stirrer at room temperature till a clear and homogeneous solution was obtained. After the reaction, NH_4OH solution was added drop wise into the stirred solution until the pH was maintained at 8.0. During this reaction the drop rate must be controlled in order to attain the chemical homogeneity. When white color precipitates were observed. The precipitate was washed with double distilled water and absolute ethanol to remove the Cl^- and NH^{4+} ions. The resulting precipitate was transferred into Teflon lined household microwave oven (2.45 GHz) with power up to 900 W and irradiated for 10 min. Same procedure was followed for preparation of pure ZnO nanopowders without use of aluminum and copper source.

2.3 Characterization techniques

The prepared nanopowders were successfully characterized by the following techniques. The crystalline structure and average grain size was analyzed by powder X-ray diffraction (XRD) using Bruker diffractometer within the 2θ range of 10°–80° using CuKα as X-ray source (k = 1.5406 Å). The particle size and surface morphology were analyzed by using transmission electron microscopy (TEM) on a Technai G20-stwin high resolution electron microscope (HRTEM) using an accelerating voltage of 200 kV. The optical transmittance of the nanopowders was recorded at room temperature by a Perkin Elmer UV/VIS/NIR Lambda 19 spectrophotometer in the wavelength range of 300–900 nm. Photoluminescence spectra of the samples were collected at room temperature by using Cary Eclipse (el02045776) Fluorescence spectrophotometer in the wavelength range of 400–800 nm with a He–Cd laser as an exciting source, and excitation wavelength of 350. The Fourier transformed infrared spectra (FT-IR) of the samples were collected using a 5DX FTIR spectrometer.

2.4 Photocatalytic experiment set up

The photocatalytic experiment on the prepared samples for the photodegradation of dyes is performed at ambient temperature. The photocatalytic activities of pure and Al–Cu–ZnO samples were evaluated by the degradation of variety of dyes, including methyl violet, phenol and rhodamine B in UV light radiation. For photocatalytic process, the dye solution was prepared by adding a particular concentration (for example 200 ml, $C_0 = 10$ mg l^{-1}) and a particular amount of synthesized material poured into the dye solution. In the experimental set up, 250 ml of water cooled cylindrical glass reactor with 125 W high pressure UV lamp was used as a light source. The samples/dye solution was irradiated in the horizontal direction and the distance between the UV lamp and the glass/dye solution was kept within 20 cm. Then the solution was kept in the dark room and well stirred with the magnetic stirrer for more than 30 min to attain the equilibrium condition throughout the solution. When the light was turned on, the experiment started. After a sudden irradiation time, the sample was taken out from the reactor. The concentration of the aqueous suspensions (methyl violet, phenol and rhodamine B) in each sample was analyzed using UV–Vis spectrophotometer at a wavelength of 664 nm. The photocatalytic efficiency was calculated from the expression $\eta = (1 - C/C_0)$, where C_0 is the concentration of dyes (methyl violet, phenol and rhodamine B) before illumination and C is the concentration of dyes after a certain irradiation time. The time interval of irradiation time was 20 min.
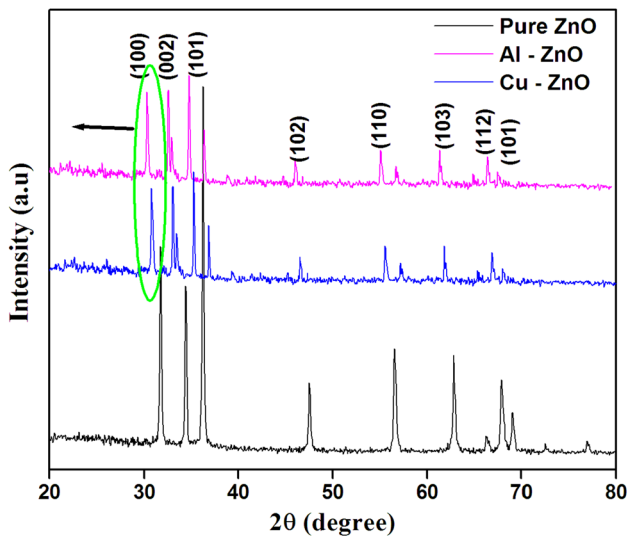
Fig. 1 Powder XRD pattern of pure ZnO, Al–ZnO and Cu–ZnO

Table 1 Shows the lattice parameters and crystallite size of ZnO, Al–ZnO and Cu–ZnO nanoparticles

Samples	Crystallite size (nm)	Lattice parameters		Cell volume ($Å^3$)
		a (Å)	b (Å)	
ZNO	24	3.2785	5.0321	54.08
Al–ZnO	18	3.2701	5.0212	53.21
Cu–ZnO	11	3.1656	5.0871	50.02

3 Results and discussion

3.1 Powder X-ray diffraction (XRD) analysis

Figure 1 shows the powder XRD pattern of pure and doped ZnO nanoparticles. In both cases, all the diffraction patterns can be indexed to the hexagonal wurtzite phase. The crystal phase of the ZnO samples agreed with the standard data of wurtzite structure (JCPDs no. 36–1451). The strongest diffraction peaks corresponding to (101), (002) and (100) plane reveals that the synthesized ZnO have samples are highly single crystalline nature. No peaks belonging to secondary phases such as Al and Cu were detected, which is confirms the purity of the samples and dopant metal ions can substitute in the regular lattice site of ZnO. Moreover pure ZnO peak position was shifted in the lower angle side and decreasing the peak intensity and also lattice parameters value (Table 1) of pure ZnO after doping of Al and Cu. This could be attributed to smaller ionic radius of Al^{3+} (0.68 Å) and Cu^{2+} (0.84 Å) than Zn^{2+} (0.88 Å).

The average crystallite size as related to the line broadening can be calculated using Scherrer's equation [18]

$$d = \frac{K\lambda}{\beta \cos\theta}$$

where d is the mean crystallite size, K is the shape factor taken as 0.89, λ is the wavelength of the incident beam, β is the full width at half maximum and θ is the Bragg angle. The calculated average crystalline size was 24, 18 and 11 nm for pure, Al and Cu doped ZnO respectively. The decrease in crystalline size of pure ZnO was attributed to dopant elements can locate at the boundary of ZnO nanoparticles, which results in decreasing the diffusion rate which prevent the growth of nanoparticles, therefore crystallite size of ZnO nanoparticles decreased. This similar phenomenon was also observed Al-doped ZnO [19].

3.2 Transmission electron microscope analysis

The surface morphology and particle size of pure and doped (Al and Cu) ZnO nanoparticles were analyzed by using TEM and the micrographs are depicts in Fig. 2. The entire TEM pictures clearly shows the samples consists of mostly spherical shaped and the average size of the nanoparticles is of the order of nanometer size. The pure ZnO nanoparticles (Fig. 2a) shows that spheroid-like shaped with large number of agglomerated particles are dominant with particle size around 25–30 nm. The average particle size was decreased 20–10 nm and also uniform and less agglomeration was observed for Al and Cu doped samples (Fig. 2b, c). This result suggests that the surface area of pure ZnO was tuned by dopant elements. The chemical compositional analysis is very important to monitor the concentration of the dopant. Figure 2d–f show that EDX spectra of undoped ZnO and Al, Cu-doped ZnO nanoparticles. It confirms the presence of Zn, O, Al and Cu elements in doped samples. Nominal percentage and chemical purity of the samples were recorded as revealed in Fig. 2d–f.

3.3 UV–Vis transmission spectra analysis

To study the electronic interactions near the optical band gap region due to the presence of dopants and to obtain the energy gap, UV–Vis transmission spectra measurements were performed on the samples in the UV–Vis region at room temperature as shown in Fig. 3. The optical transmission of Cu doped ZnO was higher than the ZnO and Al doped ZnO samples. In addition absorption edge was shifted to longer wavelength (red-shift) for Al and Cu doped ZnO samples. This may be due to decreasing the band gap energy and also surface plasmon resonance (SPR) effect. The absorbance coefficient (α) was calculated from the raw absorbance data to obtain the optical band gap (E_g). The band gap values were thus determined by the extrapolation of the linear portion of the $(\alpha h\nu)^2$ curve versus the
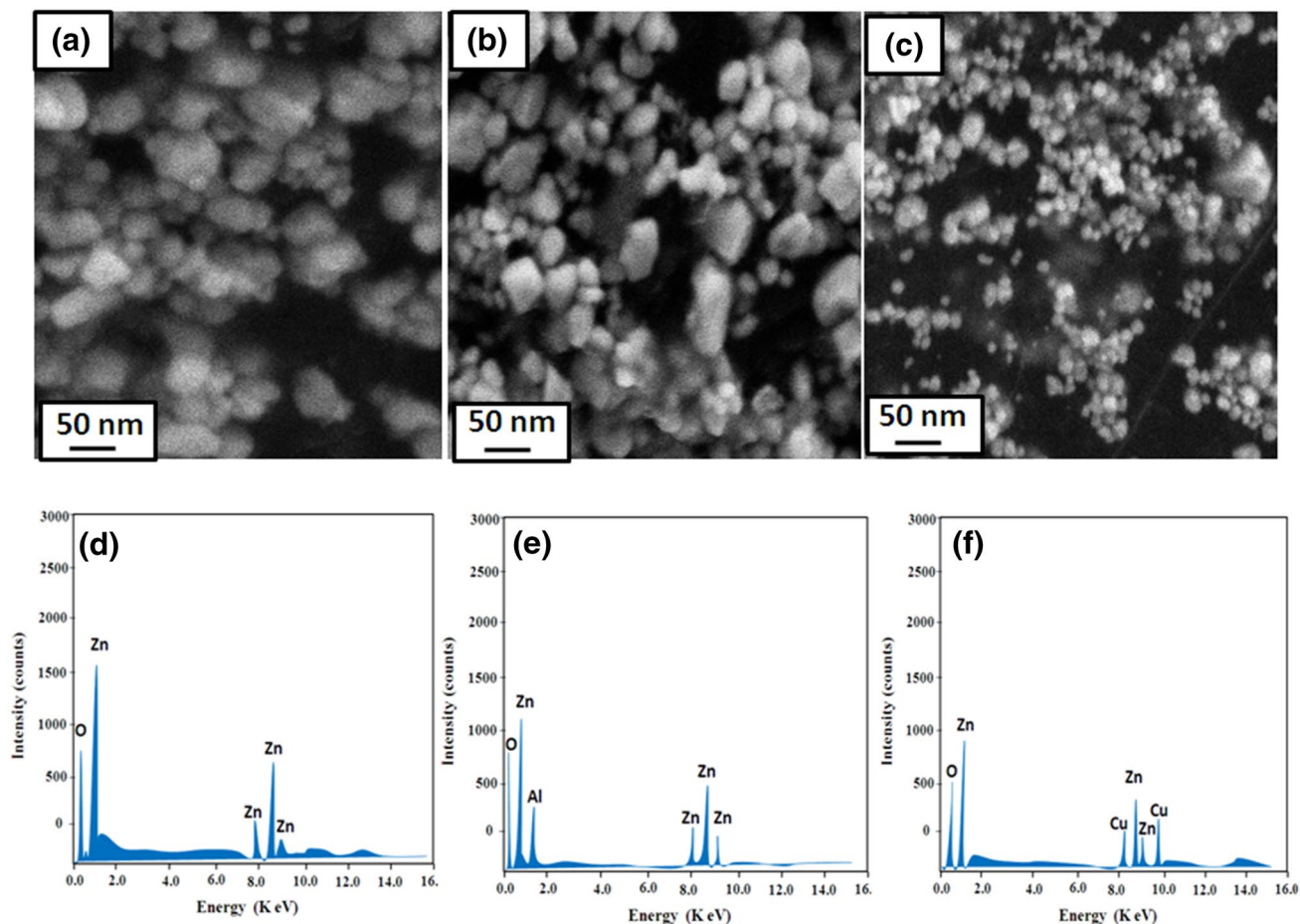
Fig. 2 TEM images of ZnO nanoparticles **a** pure ZnO, **b** Al–ZnO, **c** Cu–ZnO

photon energy hν [20]. The indirect band gap energy was found to be 3.35, 3.22 and 2.95 eV for pure, Al and Cu doped ZnO respectively. The same kind of narrowed band gap was found by Diouri et al. and enlightened by the p–d spin-exchange interactions between the band electrons and the localized d electrons of the transition-metal ion substituting the Cu^{2+} ion. Besides, the band gap drop due to doping of Cu concentration is mainly due to the strong p–d mixing of O and Cu [21].

3.4 Photoluminescence spectra analysis

Photoluminescence (PL) is one of important tool to study the structural defects and quality of crystalline structure which has been shown to play a crucial role in the development of photocatalytic property. To study the influence of Al and Cu doping on the photoluminescence of ZnO, the room temperature photoluminescence measurements were carried out (as shown in Fig. 4) at the excitation wavelength of 325 nm using He–Cd laser source. A strong UV emission at 376 nm and along with several relatively weak

visible emissions peaks were observed at 434 nm (blue emission) and 533 nm (green emission). Generally, the UV emission is attributed to free excitonic emission near band edge (NBE) [22]. The blue emission is related to transmission mediated defect such as band gap and oxygen vacancies and Zn interstitials. The green emission is peak is generally due to the oxygen vacancies, among them 533 nm is related to single oxygen (V_o^+) [23]. After doing of Al and Cu elements, the UV emission started to decrease while the green emission peak was increased, this result suggest that defect could be a crucial role in the luminescence properties of pure ZnO.

3.5 Fourier transform infrared spectra analysis (FTIR)

FTIR is a technique used to obtain information about the chemical bonding in a material. It is used to identify the elemental constituents of a material. Figure 5 shows the FTIR spectra of pure and doped ZnO samples. In pure ZnO, the vibration bands appeared at 3423 and 1596 cm^{-1}, which is related to O–H stretching vibration and O–H–O
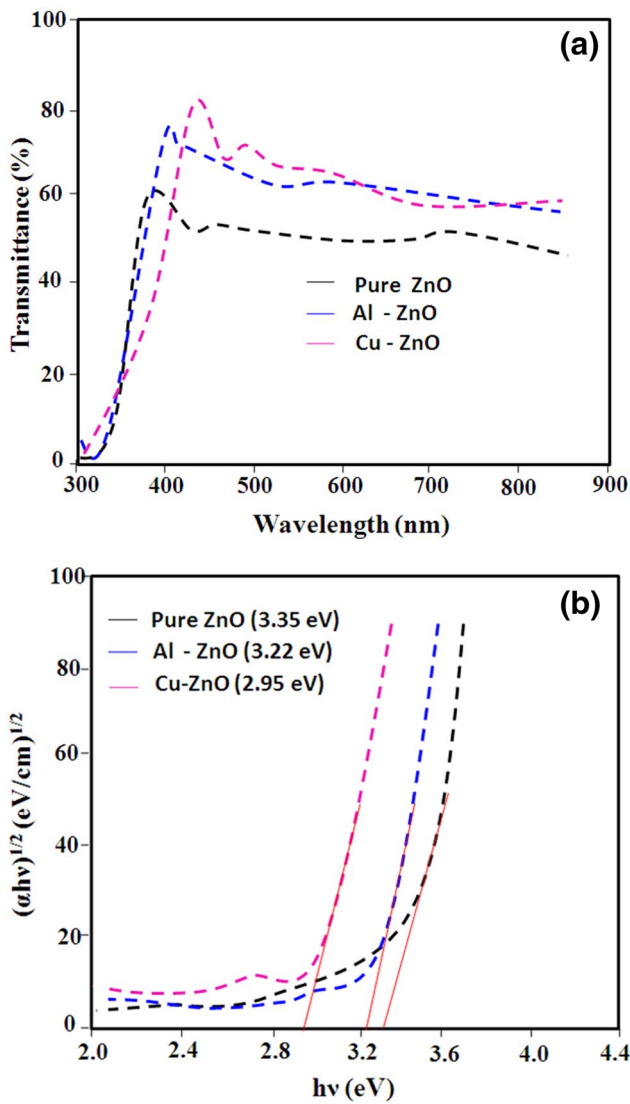
Fig. 3 UV–Vis transmission spectra of ZnO nanoparticles doped with Al and Cu content **a** transmittance spectra, **b** band gap energy plot

Fig. 4 Photoluminescence spectra of ZnO, Al–ZnO and Cu–ZnO nanoparticles
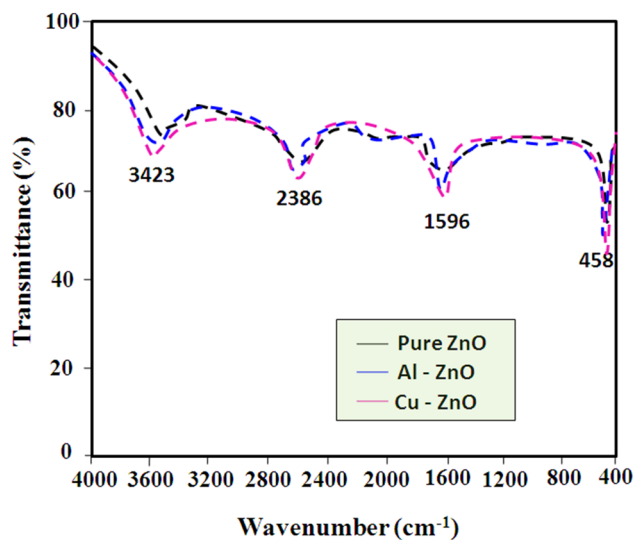
Fig. 5 FTIR spectra of ZnO, Al–ZnO and Cu–ZnO nanoparticles

bending vibration respectively [24]. The absorption peak at 2386 cm^{-1} is related to existence of CO_2 molecule present in the atmosphere [25]. The strong peak appeared at 458 cm^{-1} is related to stretching vibration of O–Zn There is no absorption peak related to O–Al and O–Cu, which is confirms the substitution of these metal ions in ZnO lattice.

3.6 Photocatalytic studies

The photocatalytic activities of ZnO, Al–ZnO and Cu–ZnO catalysts were evaluated by measuring the decomposition of various dyes such as methyl violet, phenol and rhodamine B under UV light irradiation. Figures 6, 7 and 8 show a series of absorption spectra of
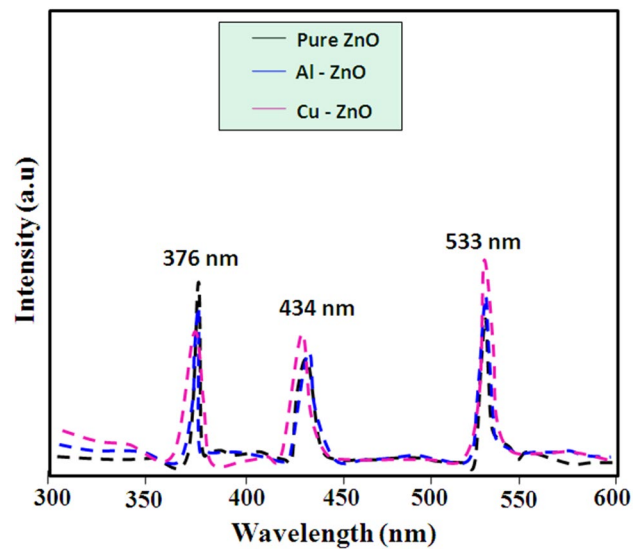
the aqueous solution of various dyes (MV, Phenol and RhB) with 10 mg of ZnO, Al–ZnO and Cu–ZnO nano photocatalysts. The degradation rates of MV under UV light after 100 min of irradiation over ZnO, Al–ZnO and Cu–ZnO were 65, 71 and 76% respectively. Similarly the Phenol and RhB degradation were 68, 73 & 78 and 69, 81 and 91% respectively. In all the cases photocatalytic efficiency was higher for Cu–ZnO catalyst than Al–ZnO and ZnO catalyst. This may be smaller band gap and high surface area of the sample. In order to further improve the photocatalytic activity recycling test was performed for degradation RhB by using Cu–ZnO catalyst under UV
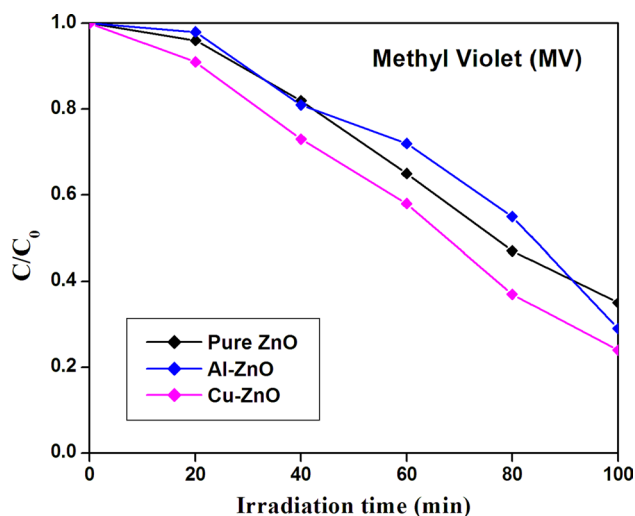
Fig. 6 Photocatalytic degradation of methyl violet using ZnO, Al–ZnO and Cu–ZnO catalyst under UV light irradiation
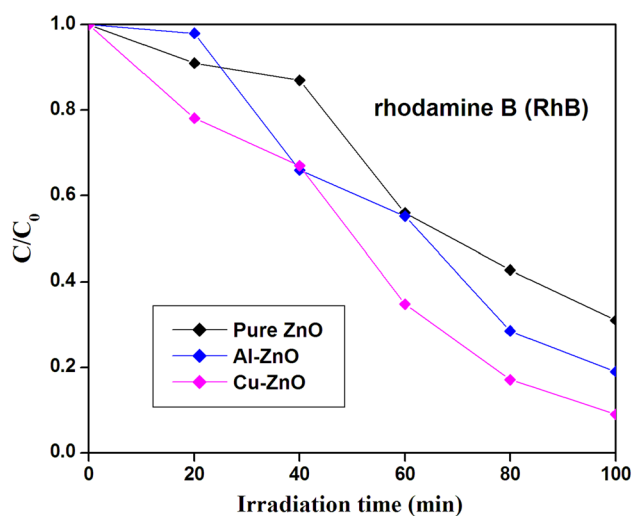

Fig. 8 Photocatalytic degradation of rhodamine B using ZnO, Al–ZnO and Cu–ZnO catalyst under UV light irradiation
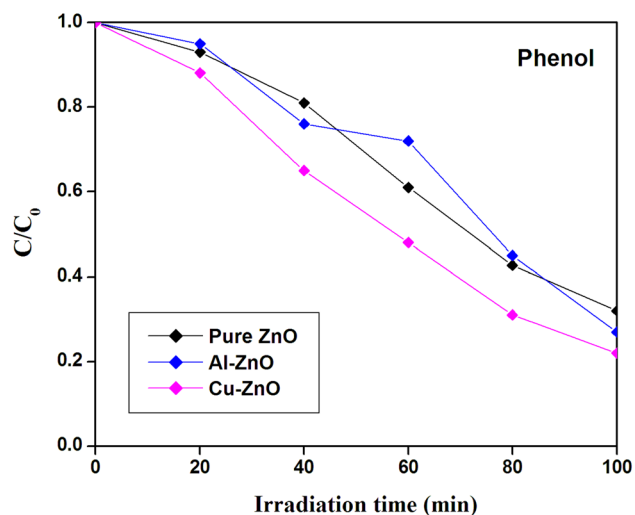

Fig. 7 Photocatalytic degradation of phenol acid using ZnO, Al–ZnO and Cu–ZnO catalyst under UV light irradiation
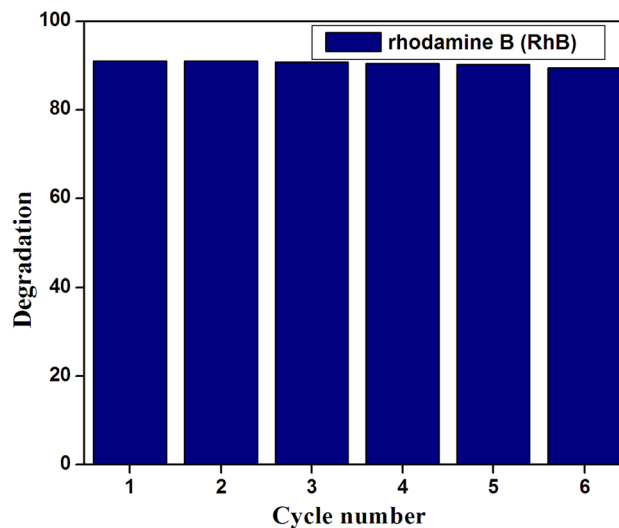

Fig. 9 Recycling test for degradation of phenol using Cu–ZnO as the photocatalyst

light irradiation and the results are shown in Fig. 9. For the reuse test, the photocatalyst was recollected by centrifuged and redispersed in the fresh dye solution followed by testing of the photocatalytic activity adopted the same procedure. After the 6 cycle testing only small variation was observed in the degradation rate. The degradation rate was found to be 91, 91, 90.8, 90.5, 90.2, 89.5% for 1–6 cycles. The insignificant variation in the photocatalytic degradation is due to the incomplete collection of the samples by the centrifugation process. Figure 10 schematically explains the photocatalytic mechanism of Al–Cu–ZnO catalysts. Generally, when semiconductor is illuminated by UV irradiation, a valence band electron

(VB) transfer to the conduction band (CB), leaving a hole in the valence band. The presence of noble metals such as Al and Cu can trapping the electron from CB of ZnO inhibits the electron–hole recombination. The noble metals (Al and Cu), acting as a trap produce more superoxide radical anion (O_2^{-*}) and at the same time VB holes of ZnO react with water to produce highly reactive hydroxyl (–OH) radical. As a result, the superoxide radical anion and hydroxyl radical are used for degradation of dyes. In our case Cu–ZnO showed high performance photocatalytic efficiency as compared to Al–ZnO and ZnO catalyst. This could be attributed to extended visible light
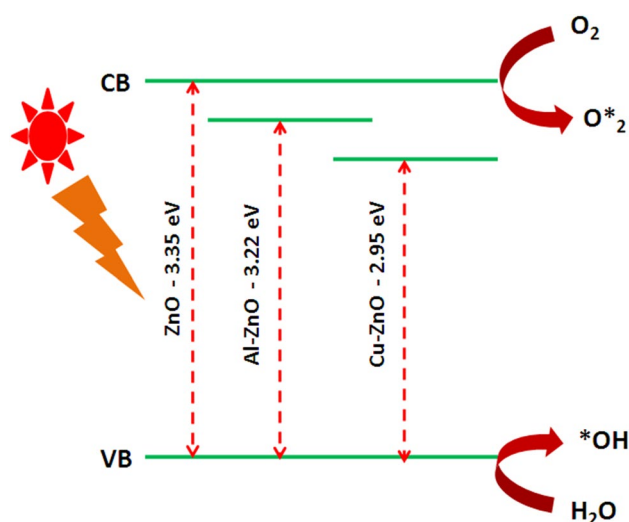
Fig. 10 Schematic representation for photocatalytic mechanism of Al–Cu–ZnO catalyst

absorption, inhibition of the electron–hole pair's recombination and enhanced adsorptivity of dye molecule on the surface of Cu–ZnO catalyst.

4 Conclusions

A novel and one step microwave approach was used to synthesis of pure and noble metals (Al and Cu) doped ZnO nano photocatalysts for the first time. The XRD and TEM results suggest that the pure phase hexagonal wurtzite type structure for both pure and doped ZnO. The decrease in lattice constants, volume, the slight shift of XRD peaks and the reduction in average crystalline size are indicated that Al and Cu has really doped into ZnO lattice. The oxygen defect and reduction band gap energy of ZnO was another crucial role in enhancing photocatalytic performance of ZnO, which is confirmed through PL studies. The highest photo degradation efficiency for rhodamine B (RhB) was attained with a catalyst ZnO loading of 5 wt.% of Cu. This improvement is an inhibition of the charge carrier recombination by Cu particles which capture photogenerated electrons. Hence this should be a promising potential catalyst for high performance photocatalytic devices.

References

1. S.G. Kumar, L.G. Devi, J. Phys. Chem. A **115**, 13211–13241 (2011)
2. J. Schneider, M. Matsuoka, M. Takeuchi, J. Zhang, Y. Horiuchi, M. Anpo, D.W. Bahnemann, Chem. Rev. **114**, 9919–9986 (2014)
3. L. Liu, X. Chen, Chem. Rev. **114**, 9890–9918 (2014)
4. S.W. Vergruggen, J. Photochem. Photobiol. C Photochem. Rev. **24**, 64–82 (2015)
5. S.G. Kumar, K.S.R.K. Rao, Appl. Surf. Sci. **355**, 939–958 (2015)
6. Z.F. Huang, J. Song, L. Pan, X. Zhang, L. Wang, J.J. Zou, Adv. Mater. **27**, 5309–5327 (2015)
7. S.G. Kumar, K.S.R.K. Rao, RSC Adv. **5**, 3306–3351 (2015)
8. L. Pan, G.Q. Shen, J.W. Zhang, X.C. Wei XC, L. Wang, J.J. Zou et al., Ind. Eng. Chem. Res **54**, 7226–7232 (2015)
9. A. Khataee, R.D.C. Soltani, Y. Hanifehpour, M. Safarpour, H.G. Ranjbar, S.W. Joo, Ind. Eng. Chem. Res. **53**, 1924–1932 (2014)
10. B. Subash, B. Krishnakumar, M. Swaminathan, M. Shanthi, Langmuir **29**, 939–949 (2013)
11. S. Kuriakose, B. Satpati, S. Mohapatra, Phys. Chem. Chem. Phys. **16**, 12741–12749 (2014)
12. C. Yu, K. Yang, W. Zhou, Q. Fan, L. Wei, J.C. Yu, J. Phys. Chem. Solids **74**, 1714–1720 (2013)
13. H. Bouzid, M. Faisal, F.A. Harraza, S.A. Al-Sayari, A.A. Ismail, Catal. Today **252**, 20–26 (2015)
14. P. Li, Z. Wei, T. Wu, Q. Peng, Y. Li, J. Am. Chem. Soc. **133**, 5660–5663 (2011)
15. Y. Liu, S. Wei, W. Gao, J. Hazard. Mater. **287**, 59–68 (2015)
16. Z.J. Wu, W. Huang, K.K. Cui, Z.F. Gao, P. Wang, J. Hazard. Mater. **278**, 91–99 (2014)
17. M. Parthibavarman, K. Vallalperuman, S. Sathishkumar, M. Durairaj, K. Thavamani, J. Mater. Sci. Mater. Electron. **25** 730–735 (2014)
18. D. Madhan, M. Parthibavarman, P. Rajkumar, M. Sangeetha, J. Mater. Sci. Mater. Electron. 26, 6823–6830 (2015)
19. Z.B. Bashi, M.H. Aslan, M. Ozer, A.Y. Oral, Cryst. Res. Technol. **44**, 961–966 (2009)
20. M. Ahmad, E. Ahmed, Y. Zhang, N.R. Khalid, J. Xu, M. Ullah, Z. Hong, Curr. Appl. Phys. **13**, 697–704 (2013)
21. M. Ferhat, A. Zaoui, R. Ahuja, Appl. Phys. Lett. **94**, 142502–142504 (2009)
22. P. Sagar, P.K. Shishodia, R.M. Mehra, H. Okada, A. Wakahara, A. Yoshida, J. Luminescen **126**, 800–806 (2007)
23. B. Guo, Z.R. Qiu, K.S. Wong, Appl. Phys. Lett. **82**, 2290–2292 (2003)
24. A.J. Reddy, M.K. Kokila, H. Nagabhushan, R.P.S. Chakradhar, C. Shivakumar, J.L. Rao, B.M. Nagabhushan, J. Alloys Compd. **509**, 5349–5355 (2011)
25. M. Arshad, A. Azam, A.S. Ahmed, S. Mollah, A.H. Naqvi, J. Alloys Comp. **509**, 8378–8381 (2011)